First-principles investigation of the structural, magnetic and electronic properties of perovskite $SrRu_{1-x}Mn_xO_3$

2009 J. Phys.: Condens. Matter 21 495501

(http://iopscience.iop.org/0953-8984/21/49/495501)

J. Phys.: Condens. Matter **21** (2009) 495501 (6pp) doi:10.1088/0953-8984/21/49/495501

First-principles investigation of the structural, magnetic and electronic properties of perovskite $SrRu_{1-x}Mn_xO_3$

L Wang[1], **L Hua and L F Chen**

Department of Physics, Nanjing Normal University, Nanjing 210097, People's Republic of China

E-mail: wanglyznj@yahoo.com.cn

Received 20 June 2009, in final form 29 August 2009
Published 12 November 2009
Online at stacks.iop.org/JPhysCM/21/495501

Abstract

We have investigated the structural, magnetic and electronic properties of single-crystal $SrRu_{1-x}Mn_xO_3$, using first-principles density functional theory within the generalized gradient approximation (GGA) + U schemes. The entire series of $SrRu_{1-x}Mn_xO_3$ ($x = 0$, 0.25, 0.5 and 1) is stabilized in the single-crystal perovskite structure which is in agreement with experimental findings. Our spin-polarized calculations give a metallic ground state for the $x < 0.5$ regime and an insulator ground state for the $x \geqslant 0.5$ regime. The magnetic structure for $x = 0$ is found to be the ferromagnetic state while the magnetic structures for $0 < x < 0.5$ are the ferrimagnetic state where any Mn ions are coupled antiparallel to the Ru at the near sites. The magnetic structures for $x \geqslant 0.5$ are found to be the antiferromagnetic states. The substitution of itinerant Ru ions by localized Mn ions enhances the p–d coupling between O and the transition metal. It also strongly drives the system from the ferromagnetic metal to the antiferromagnetic insulator.

(Some figures in this article are in colour only in the electronic version)

1. Introduction

In the past several years the ruthenates which belong to the Ruddlesden–Popper (RP) series $Sr_{n+1}Ru_nO_{3n+1}$ and $Ca_{n+1}Ru_nO_{3n+1}$ (n = number of Ru–O layers/unit cell) have been attracting considerable interest because of their intriguing physical properties, such as their diverse electronic and magnetic properties [1–3], and the unconventional superconductivity discovered in the layered ruthenate Sr_2RuO_4 [4, 5]. The $Sr_{n+1}Ru_nO_{3n+1}$ are metallic and tend to be ferromagnetic besides Sr_2RuO_4 ($n = 1$). The Curie temperature T_C for the series $Sr_{n+1}Ru_nO_{3n+1}$ increases with n, whereas the $Ca_{n+1}Ru_nO_{3n+1}$ are all on the verge of a metal–nonmetal transition and prone to antiferromagnetism. The Néel temperature T_N for the $Ca_{n+1}Ru_nO_{3n+1}$ series decreases with increasing n [6–8]. Such behavior is special and has not been observed in other transition metal RP systems. $SrRuO_3$ and $CaRuO_3$ are special cases when $n = \infty$ for the RP series [9–11]. These two compounds present the same perovskite structure with orthorhombic distortion, the same Ru^{4+} valence state, and show metallic-like resistivity. However, their magnetic properties are totally different: whilst $SrRuO_3$ is an itinerant ferromagnet, its counterpart $CaRuO_3$ magnetic ground state is paramagnetic [11].

In a recent experiment on Mn-doped $SrRuO_3$, i.e. $SrRu_{1-x}Mn_xO_3$, Cao *et al* reported that the single crystals in the limited range of compositions $0 \leqslant x \leqslant 0.6$ have shown the 3d metal Mn ion substitution for 4d Ru ions can drive the system from an itinerant ferromagnetic state for $SrRuO_3$ though a quantum critical point at $x = 0.39$ to an insulating antiferromagnetic state [12]. However, Sahu *et al* reported discrepant findings that the ferromagnetic ordering in $SrRuO_3$ is substantial up to 50% Mn substitution at the Ru site, i.e. $SrRu_{0.5}Mn_{0.5}O_3$ [13]. A more complicated phase diagram with the coexistence of ferromagnetic and antiferromagnetic phases in a wide range of substitution and a large magnetoresistance has been reported by Zhang *et al* [14]. These discrepancies have triggered extensive discussions. So,

[1] Author to whom any correspondence should be addressed.

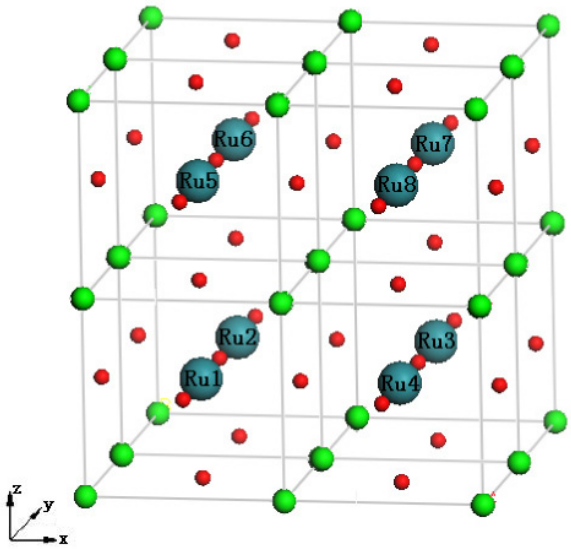

Figure 1. The supercell of the perovskite structure $SrRu_{1-x}Mn_xO_3$. The green (medium sized), blue (large sized) and red (small sized) spheres denote the Sr, Ru and O atoms, respectively. The eight different sites of Ru atoms are labeled. xyz are the local coordinates.

on the theory side, it is significant to investigate the physical properties of $SrRuO_3$ doped with Mn.

These rich varieties of physical properties relate to both the crystal structure and the character of the Ru ion. In those series of matter, the Ru ions are surrounded by O ions forming octahedra (see figure 1). The deformations and relative orientations of these corner-shared octahedra crucially determine the crystalline field splitting, the band structure, the magnetic and transport properties. Controlling the orientation of the octahedra by changing the chemical composition may systematically tune the physical properties in these materials. In these compounds, the Ru ion is also considered to be responsible for the magnetic and transport properties [15]. The major characteristic of these itinerant 4d-electron-based transition metal oxides is the extended d orbits of the Ru ion which compares to those of localized 3d ions, which greatly enhances the transition metal oxygen or p–d hybridization. Recent photoemission studies [16, 17] revealed that the spectral density of $SrRuO_3$ at the Fermi level is significantly reduced due to the strong electronic correlation. Both the strong correlation and the itinerant–localized duality of the Ru 4d electrons play important roles in the magnetic and transport properties. The strongly correlated electron systems are often characterized by competing ground states susceptible to external perturbations such as magnetic field, pressure or chemical doping. Tuning the external parameters may lead to a quantum critical point and stabilize different ground states with exotic properties. Hence, by using chemical dopants, the experimental research on RP systems has been reported widely.

One end member of the $SrRu_{1-x}Mn_xO_3$ family, $SrRuO_3$, is by far the most studied compound in the $Sr_{n+1}Ru_nO_{3n+1}$ series due to possible technological applications as an electrode material in microelectronic circuits [18]. The orthorhombic perovskite $SrRuO_3$ is an itinerant ferromagnet with $T_C \sim 165$ K and a wide range of measured saturation magnetization from 0.8 to 1.6 μ_B/Ru [19–21, 35, 37]. Moreover, this compound shows an anomalous transport property called the 'bad metal' [15, 22]. The electrical resistivity increases linearly with increasing temperature, and then passes through the Ioffe–Regel limit without saturation at high temperatures. The other end member, a cubic perovskite $SrMnO_3$, is a G-type antiferromagnet with a Néel temperature T_N of ~260 K [23, 36]. These experiments show that the perovskite $SrMnO_3$ is an insulator.

In this work, we investigate the electronic structure and magnetic property calculations of $SrRu_{1-x}Mn_xO_3$ ($0 \leqslant x \leqslant 1$) by the generalized gradient approximation (GGA) + U band structure calculations. The on-site Coulomb energy U has been taken into account to unravel the correlation effects of the localized d orbit on the magnetic moments and the electronic structures. The computational details are described in section 2. The results and discussions are presented in section 3. The conclusions are given in section 4.

2. Computational details

In terms of [12], the single crystals of the entire series of $SrRu_{1-x}Mn_xO_3$ are in the $x < 0.6$ regime. So the first-principles calculations of $SrRu_{1-x}Mn_xO_3$ with x of 0, 0.25, 0.5 and 1 are performed in a plane-wave basis set using the projector augmented wave (PAW) [24, 25] method in the generalized gradient approximation (GGA) as it is implemented in the VASP [26, 27] program. The local spin density approximation (LSDA) and GGA are known to fail in their description of the electronic properties of early transition metal (TM) compounds, as the electron self-interaction error, always present in these formulations, becomes significant for electrons in the well-localized TM d levels. Thus we have employed the DFT + U [28–31] methodology which can significantly improve predictions of phase stability and thermodynamic properties as well as magnetic and electronic structure in oxides. We use here the simple formulation by Liechtenstein *et al* [30] and Dudarev *et al* [31], where a single parameter U_{eff} determines an orbital-dependent correction to the density functional theory (DFT) energy. U_{eff} is generally expressed as the difference between two parameters, the Hubbard U, which is the Coulomb-energetic cost to place two electrons at the same site, and an approximation of the Stoner exchange parameter J, which is almost constant at 1 eV.

Since the main aim of this work is to research the structure, electronic and magnetic properties of $SrRu_{1-x}Mn_xO_3$, we have constructed a supercell consisting of 40 atoms (see figure 1). We considered all possible substituted sites and magnetic configurations for each compound and evaluated the total energy for these test structures. Using Hellmann–Feynman forces on the atoms and stresses in the unit cell, the optimization of the atomic geometry is performed via a conjugate gradient minimization of the total energy. During the simulations, atomic coordinates and axial ratios are allowed to relax for different volumes of the unit cell. These parameters are changed iteratively so that the sum of lattice energy and

Table 1. Calculated structural parameters and total magnetic moments for $SrRu_{1-x}Mn_xO_3$ ($x = 0, 0.25, 0.5, 1$).

	Composition (x)			
	0	0.25	0.5	1
a (Å)	3.996	3.959	3.869	3.851
b (Å)	3.982	3.966	3.941	3.851
c (Å)	3.986	3.948	3.934	3.851
V (Å^3)	63.43	61.99	59.98	57.11
$d_{\langle Ru-O\rangle}$ (Å)	1.993	1.980	1.874	—
$d_{\langle Mo-O\rangle}$ (Å)	—	1.975	1.934	1.926
μ_T (μ_B/f.u.)	1.95	0.50	0.00	0.00

electronic free energy converges to a minimum value. A convergence minimum with respect to atomic shifts is assumed to have been attained when the energy difference between two successive iterations is less than 10^{-7} eV/cell and the forces acting on the atoms are less than 1 meV Å^{-1}. The structure with the lowest total energy is taken as the ground state structure. For the $x = 0.25$ lattice, we replaced Ru1 and Ru6 (figure 1) by Mn, while Ru1, Ru2, Ru7 and Ru8 were substituted by Mn for $x = 0.5$. The influences of different K-point sampling and cutoff energy were explored in a series of test calculations, which led to our calculations being performed with $4 \times 4 \times 4K$-point sampling and with the basis set for valence electrons consisting of plane waves with a cutoff energy of 520 eV. To explore the effects of the on-site Coulomb energy U on the electronic structures and the magnetic moments, specific values for Ru ($U = 1.0$ eV and $J = 0.9$ eV) and Mn ($U = 5.0$ eV and $J = 0.9$ eV) are used in the GGA + U calculation. We tested the value of U from 0 to 10 eV for Ru and Mn. We found that the magnetic moment deviated from the experiment when we selected larger values of U. On the other hand, the $SrRu_{0.5}Mn_{0.5}O_3$ compound is the metal ground state, which is in contradiction to the experiment, when we selected smaller values of U.

3. Results and discussion

3.1. Structure relaxation

We show our calculated relaxed structural parameters for different compositions by using the GGA + U method in table 1. The unit cell shape, lattice vectors and atomic coordinates are optimized simultaneously during optimizing. The single-crystal structure of the compound for $x = 1$, i.e. $SrMnO_3$, has a cubic lattice with $Pm\bar{3}m$ group, while the single-crystal structure of the compound for $x = 0$, $SrRuO_3$, is an orthorhombic lattice with $Pbnm$ group. It is in good agreement with the experimental result of the single-crystal $SrRu_{1-x}Mn_xO_3$ [12], but differs from polycrystalline $SrRu_{1-x}Mn_xO_3$. Recently, Kolesnik *et al* reported that polycrystalline $SrRu_{1-x}Mn_xO_3$ for $0.3 \leqslant x \leqslant 0.7$ were a tetragonal structure [32]. The discrepancy may be explained by the difference between the single crystal and polycrystalline. From table 1, we can find that the cell volume decreases over the entire range of compositions. Synchronously, the mean bond distance $d_{\langle Ru-O\rangle}$ decreases from 1.993 Å for $x = 0$ to 1.874 Å for $x = 0.5$. The mean bond distance $d_{\langle Mn-O\rangle}$ decreases from 1.975 Å for $x = 0.25$ to 1.926 Å for $x = 1$. The relaxed bond angle of Ru–O–Ru is 171° in the $SrRuO_3$ compound. The bond angles of Ru–O–Ru Mn–O–Mn and Ru–O–Mn are almost 180° in the other $SrRu_{1-x}Mn_xO_3$ compounds. The lattice parameters, the cell volume and the bond distances systematically decrease with increasing x because the ionic radius of Mn^{4+} (0.53 Å) is smaller than that of Ru^{4+} (0.62 Å). Otherwise, we have found that the shrinking in the a and c axes is more rapid with increasing x. This distinct behavior is accompanied by drastic changes in the electronic and magnetic structure. According to the Vegard law [33], the volume would be expected to vary linearly with changing x. So we plot the variation of the unit cell volume V as a function of composition x in figure 2 (remembering that the GGA [34] is likely to overestimate the volume by 2%–3%). The variation of V over the range of compositions ($0 \leqslant x \leqslant 1$) studied here is almost linear with the composition x.

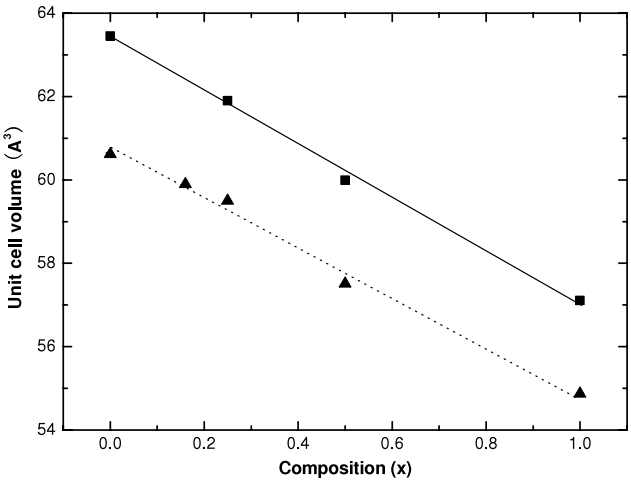

Figure 2. Calculated unit cell volume V (solid square) as a function of the composition x compared with the experimental ones (solid triangle). The experimental data are taken from [12, 23].

3.2. Electronic structure

The spin-polarized GGA + U calculations give a metallic ground state at $x = 0$ and 0.25 and an insulator ground state at $x = 0.5$ and 1 in $SrRu_{1-x}Mn_xO_3$, which are in agreement with experiments [12]. In figures 3(a)–(d), we show the calculated total density of states (DOS) of $SrRu_{1-x}Mn_xO_3$ and partial Ru 4d, Mn 3d and O 2p DOS for different compositions. For our discussion of the density of states, which is limited to an energy window of −8 to about 4 eV, we shall be primarily concerned with the Ru d, Mn d and O p states, since the Sr-derived states appear higher in energy. $SrRuO_3$, i.e. the composition $x = 0$ (see figure 3(a)), is known to be a ferromagnetic metal, which is consistent with our DOS calculation. The O 2p bands span from ∼7.7 below the Fermi level (E_F) to ∼4 eV above the Fermi level, while the main peaks of spin-up and spin-down Ru t_{2g} bands are located at ∼0.4 eV below and ∼0.5 eV above the Fermi level, respectively. Meanwhile, the Ru bands near E_F (from about −0.8 to 1.3 eV) are composed of t_{2g} and e_g,

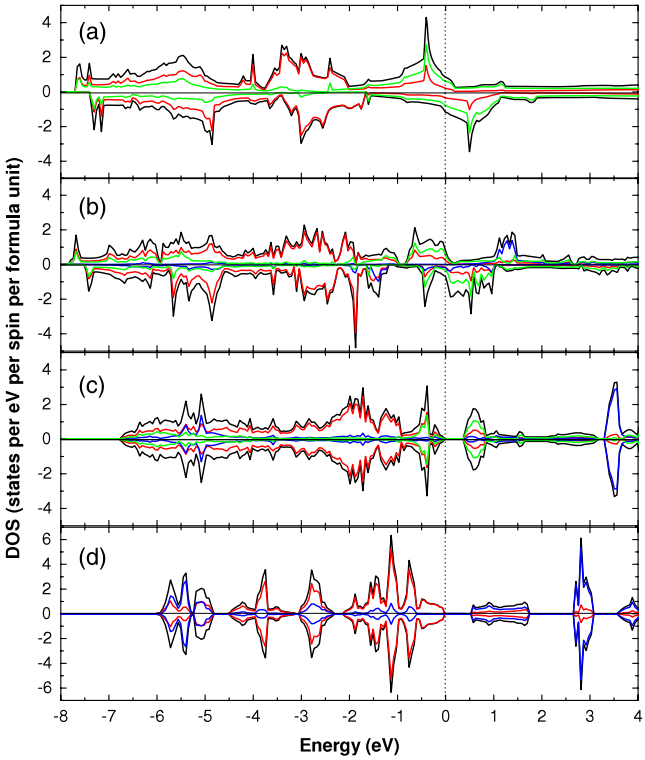

Figure 3. Total (black line) densities of states and partial densities of states of Ru 4d (green line), O 2p (red line) and Mn 3d (blue line) in $SrRu_{1-x}Mn_xO_3$ using the GGA + U method. The energy zero is taken at the Fermi level. The upper halves of each panel display the spin-up states and the lower halves spin-down states.

in which the spin-up and spin-down bands are mainly made up by e_g and t_{2g}, respectively. The bands from 1.3 eV to higher energy above the Fermi level are dominated by Ru e_g and O 2p in both spin channels. The spin-down Ru t_{2g} and e_g bands pass the Fermi level from below E_F to unoccupied bands, while the spin-up Ru t_{2g} bands entirely cross the Fermi level, resulting in a metallic ferromagnetic ground state.

For $x = 0.25$ (see figure 3(b)), the spin-up and spin-down conduction bands crossing the Fermi level are dominated by the admixture of Ru t_{2g}, Mn t_{2g} and oxygen p states. The generic features of the DOS for $x = 0.25$ show metal character. We can find the occupied DOS of Mn is almost in the spin-down channel. Such a display is in accordance with the Mn magnetic configuration (see section 3.3). Obviously, several very sharp peaks which appear in the channel below the Fermi level (from about -0.7 to -0.1 eV) are made up by the Ru 4d, O 2p and Mn 3d, which is associated to the enhanced coupling of those ions p–d states. Otherwise, the obvious peaks between 1.8 and 5.4 eV below the Fermi level are mainly composed of O p states.

With a further increase of Mn atoms, the DOS of the compositions change inevitably. For $x = 0.5$, since the residual Ru ions are relatively far away from each other, all the bandwidths are noticeably suppressed (see figure 3(c)) due to the reduced overlaps among the electron clouds. Hence, a crystal field energy gap at E_F is cut down between the occupied Ru, Mn t_{2g} and unoccupied Ru, Mn e_g bands, giving rise to an insulator ground state with energy gaps of 0.5 eV. Figure 3(c) illustrates that these peaks are all composed of Ru d, Mn d and O p, which elucidates that the p–d hybridization is more enhanced. The bands between 1 and 4.6 eV below E_F are mainly made up by the O p state. The peak at ∼3.5 eV above E_F is mainly dominated by Mn e_g states. The bandwidth suppression is clear in the insulator $x = 1$ case which has energy gaps of 0.64 eV (see figure 3(d)). The last two figures both have symmetrical DOS between spin-up and spin-down bands, hence these compositions are antiferromagnetic states. In figure 3, with increasing x, a substantial enhancement is obtained for the p–d coupling of the O 2p and the Mn 3d, Ru 4d states which are associated with the decrease of Mn–O and Ru–O bonds. The decrease of bond length has the effect of enhancing the hybridization matrix element. It causes the change of physical character.

Table 2. The atoms in the parentheses show the sites where Ru atoms were replaced. The third and fourth columns give the nearest and the next-nearest number of Mn and/or Ru neighbors. The last column give the magnetic moment at various inequivalent sites.

x	Sites	nn	nnn	Magnetic moment (μ_B)
0	Ru	6Ru	12Ru	1.462
0.25	Mn1(Ru1)	6Ru	4Mn + 8Ru	−2.978
	Ru2	4Mn + 2Ru	12Ru	1.330
	Ru3	6Ru	8Mn + 4Ru	1.053
	Ru4	2Mn + 4Ru	12Ru	1.249
	Ru5	4Mn + 2Ru	12Ru	1.330
	Mn2(Ru6)	6Ru	4Mn + 8Ru	−2.978
	Ru7	2Mn + 4Ru	12Ru	1.249
	Ru8	6Ru	8Mn + 4Ru	1.053
0.5	Mn1(Ru1)	2Mn + 4Ru	4Mn + 8Ru	−3.774
	Mn2(Ru2)	2Mn + 4Ru	4Mn + 8Ru	3.774
	Ru3	4Mn + 2Ru	8Mn + 4Ru	−1.546
	Ru4	4Mn + 2Ru	8Mn + 4Ru	1.546
	Ru5	4Mn + 2Ru	8Mn + 4Ru	1.546
	Ru6	4Mn + 2Ru	8Mn + 4Ru	−1.546
	Mn3(Ru7)	2Mn + 4Ru	4Mn + 8Ru	3.774
	Mn4(Ru8)	2Mn + 4Ru	4Mn + 8Ru	−3.774
1	Mn	6Mn	12Mn	±3.032

In figure 3(a), the 4d t_{2g} orbit in $SrRuO_3$ is itinerant due to self-doping by the O 2p electrons and the system is metallic. In figures 3(b) and (c), relative itinerant Ru ions are substituted by localized Mn ions. The metallic character disappears gradually since the first and second nearest neighbors are more and more Mn ions (see table 2) and electron hopping between conductive Ru ions is therefore unavailable in the doping process. Under the octahedral crystal field, the four 4d electrons of the Ru^{4+} ion occupy the t_{2g} triplet and leave the higher e_g doublet empty, hence a low spin state with $S = 1$ ($t_{2g}^3\uparrow$, $t_{2g}^1\downarrow$). The total spin of Mn^{4+} is $S = 3/2$ ($t_{2g}^3\uparrow$). In the doping process, the substitution of Ru^{4+} by Mn^{4+} eliminates one of the t_{2g} electrons and hence the itinerant character of the d electrons. The Mn t_{2g} levels are all occupied with one electron, the only possibility of hopping would be to temporarily fill one of the e_g levels. This process is energetically unfavorable. As a consequence of the large crystalline field splitting in the MnO_6 octahedra (see figure 3(d)), the Mn sites interrupt the dynamics of the

4d t_{2g} electrons, and the metallic character of the compounds gradually disappears, then the insulator character appears.

3.3. Magnetic properties

The calculated total magnetic moments (μ_T) for $SrRu_{1-x}Mn_xO_3$ are listed in table 1. The magnetic structure for $x = 0$ is found to be the ferromagnetic (FM) state and the FM state is 0.19 eV lower than the paramagnetic state. The magnetic structure for $x = 0.25$ is the ferrimagnetic (FIM) state where the Mn spins are aligned antiferromagnetically at the sites that the Mn ions occupied in the Ru ions (see figure 1). This FIM state is 0.25 eV lower in energy than the constrained FM solution. The μ_T shows the remarkable decrease from 1.95 μ_B for $x = 0$ to 0.5 μ_B for $x = 0.25$, which is consistent with the experiment [12]. The magnetism arises from strongly hybridized itinerant Ru–O bands, leading to substantial O contributions to the moment. It may affect the fit of neutron scattering data so our calculated moment of $SrRuO_3$ is a little higher than the experimental values of [12], but it is quite consistent with other experiments [19–21]. The magnetic structure for $x = 0.5$ and 1 is the antiferromagnetic (AFM) state where each atom is aligned antiferromagnetically with the nearest-neighbor Ru/Mn atoms, which agrees with the [12] findings that $SrRu_{1-x}Mn_xO_3$ has an antiferromagnetical magnetic structure in the $x \geqslant 0.39$ regime. For $x = 1$, $SrMnO_3$, the FM state is 1.01 eV higher than the AFM state. $SrMnO_3$ is the AFM ground state. So we tested three types of AFM structures and found the G-type AFM is 0.61 eV and 0.23 eV lower than the A-type and C-type AFM structures, respectively. In the ferrimagnetic regime, as the Mn content increases, we find a rapid decrease of μ_T. This is readily understood as Mn atoms are all surrounded by Ru atoms due to low Mn concentration. The Mn 3d electrons are local and Mn ions are connected to the next Ru by 180° Mn–O–Ru bonds and, consequently, being antiferromagnetically coupled. In the Mn-rich regime ($x \geqslant 0.5$) where more Mn ions surround Ru ions, $SrRu_{1-x}Mn_xO_3$ becomes the antiferromagnetic magnetic structure so the total magnetic moments $\mu_T = 0$.

As table 2 shows the magnetic moments of inequivalent Ru and Mn (labeled in figure 1), the number of Ru and Mn atoms in various neighboring shells differ from that of the ordered arrangement. We notice that magnetic moments of Ru ions surrounded by more Mn ions are bigger than those surrounded by less Mn in the $x = 0.25$ regime. The increase of the absolute magnetic moment of Ru and Mn from $x = 0.25$ to 0.5 may be explained by the strong antiferromagnetic (AFM) super-exchange interaction between the nearest sites of atoms. Our calculations show that the difference between $SrRu_{1-x}Mn_xO_3$ and $SrRuO_3$ is the fact that the crystal field gap between the t_{2g} and the e_g levels plays a key role, for the crystal field gap is irrelevant. With doping Mn the coupling of O 2p, Ru 4d and Mn 3d is substantially enhanced. The enhanced p–d coupling will increase the effective hopping strength. Thus, the antiferromagnetic coupling between adjacent atoms is strengthened. Consequently, Mn doping will reinforce the antiferromagnetic interaction and $SrRu_{1-x}Mn_xO_3$ compositions change from the ferromagnetic state to the antiferromagnetic state with x increasing.

4. Conclusions

In conclusion, we investigate a study of the structural, electronic and magnetic properties of the single-crystal $SrRu_{1-x}Mn_xO_3$ with x of 0, 0.25, 0.5 and 1 using first-principles density functional theory within the generalized gradient approximation (GGA) + U schemes. The crystal structures of the compounds change from an orthorhombic lattice for $x = 0$ to a cubic lattice for $x = 1$. It is interesting to note that the variation of V over the range of compositions ($0 \leqslant x \leqslant 1$) studied here is linear with composition x. Our spin-polarized calculations give a metallic ground state for the $x = 0$ and 0.25 regimes and an insulator ground state for the $x \geqslant 0.5$ regimes. The magnetic structure for $x = 0$ is found to be the ferromagnetic state. The magnetic structure for $x = 0.25$ is the ferrimagnetic state where any Mn at the Ru crystallographic site is coupled antiparallel to the Ru moments at the adjacent site. The magnetic structure for $x \geqslant 0.5$ is the antiferromagnetic state where each atom is aligned antiferromagnetically with the nearest-neighbor atoms. With Mn doping, the p–d coupling between O and the transition metal is substantially enhanced. Synchronously, the substitution of itinerant Ru ions by localized Mn ions strongly drives the system from the ferromagnetic metal to the antiferromagnetic insulator.

Acknowledgments

Numerical calculations were carried out using the facilities of the Department of Physics in Nanjing Normal University.

References

[1] Itoh M, Shikano M and Shimura T 1995 *Phys. Rev.* B **51** 16432
[2] Mazin I I and Singh D J 1999 *Phys. Rev. Lett.* **82** 4324
[3] Durairaj V, Chikara S, Lin X N, Douglass A, Cao G, Schlottmann P, Choi E S and Guertin R P 2006 *Phys. Rev.* B **73** 214414
[4] Mazin I I and Singh D J 1997 *Phys. Rev. Lett.* **79** 733–6
[5] Maeno Y, Hashimoto H, Yoshida K, Nishizaki S, Fujita T, Bednorz J G and Lichtenberg F 1994 *Nature* **372** 532
[6] Grigera S A, Perry R S, Schofield A J, Chiao M, Julian S R, Lonzarich G G, Ikeda S I, Maeno Y, Millis A J and Mackenzie A P 2001 *Science* **294** 329
[7] Puchkov A V, Schabel M C, Basov D N, Startseva T, Cao G, Timusk T and Shen Z-X 1998 *Phys. Rev. Lett.* **81** 2747
[8] Crawford M K, Harlow R L, Marshall W, Li Z, Cao G, Lindstrom R L, Huang Q and Lynn J W 2002 *Phys. Rev.* B **65** 214412
[9] Cao G, McCall S, Shepard M, Crow J E and Guertin R P 1997 *Phys. Rev.* B **56** 321
[10] Yoshimura K, Imai T, Kiyama T, Thurber K R, Hunt A W and Kosuge K 1999 *Phys. Rev. Lett.* **83** 4397
[11] Mukuda H, Ishida K, Kitaoka Y, Asayama K, Kanno R and Takano M 1999 *Phys. Rev.* B **60** 12279
[12] Cao G, Chikara S, Lin X N, Elhami E and Durairaj V 2005 *Phys. Rev.* B **71** 035104
[13] Sahu R K, Hu Z, Rao M L, Manoharan S S, Schmidt T, Richter B, Knupfer M, Golden M, Fink J and Schneider C M 2002 *Phys. Rev.* B **66** 144415
[14] Zhang X-Y, Chen Y, Li Z-Y, Vittoria C and Harris V G 2007 *J. Phys.: Condens. Matter* **19** 266211

[15] Allen P B, Berger H, Chauvet O, Forro L, Jarlborg T, Junod A, Revaz B and Santi G 1996 *Phys. Rev.* B **53** 4393
[16] Fujioka K, Okamoto J, Mizokawa T, Fujimori A, Hase I, Abbate M, Lin H J, Chen C T, Takeda Y and Takano M 1997 *Phys. Rev.* B **56** 6380
[17] Okamoto J, Mizokawa T, Fujimori A, Hase I, Nohara M, Takagi H, Takeda Y and Takano M 1999 *Phys. Rev.* B **60** 2281
[18] Eom C B, Cava R J, Fleming R M, Phillips Julia M, vanDover R B, Marshall J H, Hsu J W P, Krajewski J J and Peck W F Jr 1992 *Science* **258** 1766
[19] Callaghan A, Moeller C W and Ward R 1966 *Inorg. Chem.* **5** 1572
[20] Longo J M, Raccah P M and Goodenough J B 1968 *J. Appl. Phys.* **39** 1327
[21] Kanbayasi A 1976 *J. Phys. Soc. Japan* **41** 1876
Kanbayasi A 1978 *J. Phys. Soc. Japan* **44** 89
Kanbayasi A 1978 *J. Phys. Soc. Japan* **44** 108
[22] Gunnarsson O, Calandra M and Han J E 2003 *Rev. Mod. Phys.* **75** 1085
[23] Takeda T and Ohara S 1974 *J. Phys. Soc. Japan* **37** 275
[24] Blöchl P E 1994 *Phys. Rev.* B **50** 17953
[25] Kresse G and Joubert D 1999 *Phys. Rev.* B **59** 1758
[26] Kresse G and Furthmuller J 1996 *Phys. Rev.* B **54** 11169
[27] Kresse G and Furthmuller J 1996 *Comput. Mater. Sci.* **6** 15
[28] Anisimov V I, Zaanen J and Andersen O K 1991 *Phys. Rev.* B **44** 943
[29] Rohrbach A, Hafner J and Kresse G 2003 *J. Phys.: Condens. Matter* **15** 979
[30] Liechtenstein A I, Anisimov V I and Zaanen J 1995 *Phys. Rev.* B **52** R5467
[31] Dudarev S L, Botton G A, Savrasov S Y, Humphreys C J and Stutton A P 1998 *Phys. Rev.* B **57** 1505
[32] Kolesnik S, Dabrowski B and Chmaissem O 2008 *Phys. Rev.* B **78** 214425
[33] Denton A R and Ashcroft N W 1991 *Phys. Rev.* A **43** 3161
[34] Häussermann U, Blomqvist H and Noréus D 2002 *Inorg. Chem.* **41** 3684
[35] Rondinelli J M, Caffrey N M, Sanvito S and Spaldin N A 2008 *Phys. Rev.* B **78** 155107
[36] Sødenå R and Ravindran P 2008 *Phys. Rev.* B **74** 144102
[37] Mahadevan P, Aryasetiawan F, Janotti A and Sasaki T 2009 *Phys. Rev.* B **80** 035106